On Effect of Cell Base Width on Thrust Performance of a Scramjet External Nozzle

T. Isono[1]*

1: Research and Development Directorate, Japan Aerospace Exploration Agency, Japan

* Correspondent author: isono.tatsushi@jaxa.jp

Abstract

The present study experimentally investigated the effect of cell base width on the thrust performance of the Scramjet External Nozzle (SEN) and computationally expressed those effect, based on the wind tunnel test. The cell base structure divides each engine module. Three test models were employed of which shape differs from each other. One is not clustered configuration, while the others are clustered and each of them has a different cell base width. The experimental study showed that the nozzle wall pressure distribution is altered corresponding to the cell base width and the under expansion condition is more sensibly affected by cell base width than over expansion condition. Additionally, the input correction is proposed to reflect the clustering effect to the computation model, which unifies the input physical quantities by solving mass, streamwise momentum, and energy conservation equations.

Keyword: *Wind Tunnel Test, Nozzle Flow, Scramjet External Nozzle (SEN), Engine Clustering, Cell Base Width*

1. Introduction

A hypersonic airbreathing engine like scramjet is one of the key technologies to realize Reusable Launch Vehicle (RLV) [1]. Due to efficient Airframe-Propulsion Integration (PAI) [2], the engine should be equipped to the underbelly of the airframe fuselage in integrating manner. In such a configuration, the rear bottom surface of airframe is utilized as the nozzle expansion wall. The lower side wall of this nozzle, called cowl, is truncated to reduce the system weight, friction loss, and heat load. This type of nozzle is called Scramjet External Nozzle (SEN) [3]. The “external” means that one side of the nozzle flow is opened to the atmosphere that is external environment due to cowl truncation.

Meanwhile, for maintainability and operability, a scramjet engine should be modularized so that the combustor exit, viz. nozzle entrance, is clustered across the cell bases. The cell base width varies with respect to the clustering manner which is affected by combustor unit layout. The exhausts issuing from neighboring combustor units shape the wale flow across the cell base. The size of large-scale separation bubbles shaped by wake flow is changed with the cell base widths, so that also the drag produced by the cell base should vary. Final goal of our research series for SEN is to develop the performance prediction tool which can derive the SEN thrust performances quickly and accurately enough for conceptual design phase. The present study experimentally evaluated the impact of cell base width on SEN thrust performance and discussed the methodology applying the existence of cell base with width variation to performance prediction tool. Note that the effects of ambient flow and fixed-scale cell base existence had been characterized in the previous studies [4, 5].

2. Experimental Approach

2.1 Wind tunnel facility and test model

The wind tunnel test had been carried out using the long-duration blow-down facility called Pilot Wind Tunnel (PWT) located on Kakuda Space Center (KSPC), Japan Aerospace Exploration Agency (JAXA). Since the present test objective was on the aerodynamic characterization, room-temperature nitrogen and dry air were

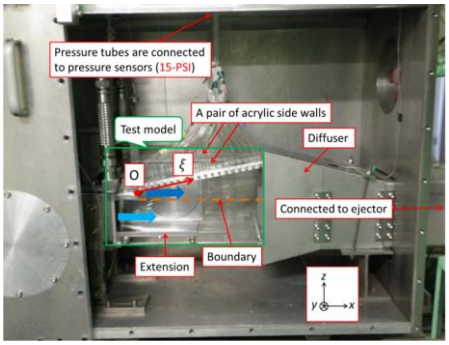

Fig. 1 Side view photograph of test chamber

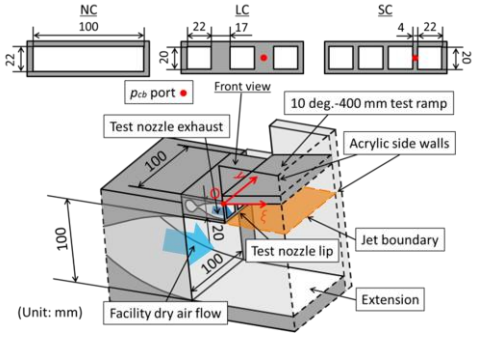

Fig. 2 Schematic for test model

Table 1 Specification of test nozzle

Test nozzle kind	NC	LC (1 set)	SC (1 set)
Number of flow paths	1	3	4
Cell base to flow path widths	-	17/22	4/22
Throat shape	100 mm x 2.95 mm	2.95 mm x 20 mm	2.95 mm x 20 mm
Flow path exit shape	100 mm x 22 mm	22 mm x 20 mm	22 mm x 20 mm
Expansion ratio	22/2.95	22/2.95	22/2.95
Expansion direction	Height (z)	Width (y)	Width (y)

employed as working gas. In other words, the reactive and thermodynamical features were not addressed in the present paper. This facility is categorized in the supersonic free-jet type, so that it has a large-scale depressurized test chamber relative to the test model. Figure 1 is the lateral view photograph inside the test chamber. The facility nozzle and diffuser are inserted into the test chamber from left and right side walls in Fig. 1. The diffuser is connected to facility ejector which depressurizes the test chamber from 7.0 to 12.0 kPa. The nozzle flow to be observed was configured between the facility nozzle and diffuser, which is enclosed by green square in Fig. 1.

Figure 2 is the schematic for the test model. The facility nozzle has a square shaped exit with 100 mm x 100 mm measurement. The test nozzle was installed in the facility nozzle exit. The bottom side outer wall of the test nozzle was connected smoothly to the upper side inner wall of the facility nozzle. The Mach 2.0 dry air and Mach 3.5 nitrogen flows issued from the facility and test nozzles, respectively. These Mach numbers were so selected that the observed flow kept fully supersonic throughout the test model under constraints from facility specification. Three test nozzles were employed, whose exit configurations differ from each other. One is not clustered configuration, while the others are clustered and each of them has a different cell base width. The test nozzle specifications are summarized in Table 1, and the dimensions of each nozzle exit are also written in upper side sketches in Fig. 2. Non clustered test nozzle is called No-Cell (NC) base case, whereas clustered ones are called Larger-Cell (LC) base and Smaller-Cell (SC) base cases respectively. The test ramp was assembled to the test nozzle. The bottom wall of test ramp was continuously connected to the upper side inner wall of the test nozzle. The facility and test nozzle flows simulated ambient flow and engine exhaust, respectively. The test ramp simulated the SEN ramp wall, that is, thrust generating surface. The components correspondence of experimental setup to actual engine system is given in Tabel 2.

2.2 Test condition

The dimensionless parameter of Nozzle Pressure Ratio (*NPR*) for test nozzle was employed as a test parameter defining test conditions, which determines the expansion condition of nozzle flow. For the present test configuration, the *NPR* was defined as the ratio of the test nozzle total to facility nozzle exit pressures. The facility nozzle exit pressure was regarded as ambient flow pressure. The test nozzle total and ambient flow pressures were symbolized as p_{0n} and p_a, respectively.

Due to test nozzle exit Mach number of 3.5, the optimum *NPR* can be theoretically derived as 76. In the case of *NPR* completely equal to the optimum value of 76, the test nozzle exhaust takes the optimum expansion condition where no waves form at the interaction beginning point with the ambient flow. The interaction beginning point is located at the trailing edge of the bottom side wall of test nozzle. For actual engine system, this point corresponds to the cowl trailing edge generally called cowl lip, so that we called this point the test

Table 2 Components correspondence

Experiment	Actual engine system
Test nozzle exhaust	Engine exhaust
Facility nozzle exhaust	Ambient flow
Test ramp	SEN ramp wall
Test nozzle lip	Cowl lip
Rectangle side wall	Side fence

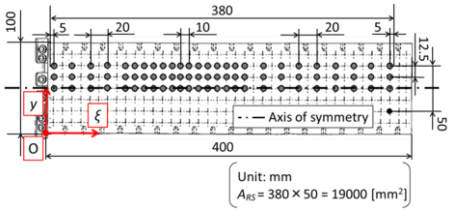

Fig. 3 Measurement location on test ramp surface

nozzle lip in the present study (see Table 2). For the *NPR* less than 76, this case is called over expansion condition where the shock and expansion waves emanate from the test nozzle lip to test nozzle exhaust and ambient flow, respectively. Inversely, in the case that the *NPR* is larger than 76, the expansion and shock waves emerge from the test nozzle lip to test nozzle exhaust and ambient flow, respectively. This case is called under expansion condition. We arranged the *NPR* range as wide as possible by controlling p_{0n} and p_a within facility limitation, and then the experimental results were compared in the cases having close *NPR*.

2.3 Measurement and data reduction

Surface pressure measurement was applied to the cell base and test ramp, to characterize the SEN thrust performance with variation in cell base width. The cell base pressure p_{cb} was measured at red dot location described in test nozzle exit sketch in Fig. 2. The wall pressure p_w distribution was two-dimensionally measured. The pressure measurement location on test ramp surface is illustrated in Fig. 3. The flow symmetry allowed to measure one side of test ramp surface from symmetrical line. We employed the continuous multi-point pressure measurement system called 15-PSIESP-64-HD manufactured by Pressure Systems Inc., which ranges from 0 to 100 kPa. The sampling frequency was 10 Hz, and the time history of measurement value was averaged in 1.0 s for giving comparison results.

The two-dimensional wall pressure distribution on test ramp should be dominated by pressure wave pattern forming in test nozzle exhaust [4], and the expansion condition defined by *NPR* determined the pressure wave pattern. Aiming to develop a performance prediction model with reduced order concept, one-dimensional pressure distribution was also defined through spatial averaging, which is called Spanwise Averaged Pressure Distribution (SAPD). The SAPD was derived from the following equations,

$$\begin{cases} y_j = 75 - 12.5(j-1) \\ \left(\dfrac{p_{wave}}{p_{0n}}\right)(\xi) = \dfrac{1}{p_{0n}}\left\{\dfrac{1}{5}\cdot\sum_{j=1}^{5} p_w(\xi, y_j)\right\} \end{cases} \tag{1}$$

where y, and ξ mean the spanwise and streamwise coordinates on the test ramp, respectively, and j indicates the pressure measurement location in spanwise allocated. First and second equations mean the spanwise coordinate and ramp wall pressure normalization by test nozzle total pressure and spanwise averaging to acquire one-dimensional distribution, respectively. To express the spanwise pressure variation in one-dimensional distribution, the standard deviation was also calculated as follows, and it gives the error bar in one-dimensional pressure distribution graph.

$$\sigma_y(\xi) = \sqrt{\frac{1}{5}\cdot\sum_{j=1}^{5}\left\{\left(\frac{p_w}{p_{0n}}\right)(\xi, y_j) - \left(\frac{p_{wave}}{p_{0n}}\right)(\xi)\right\}^2} \tag{2}$$

The pressure coefficient C_p representing dimensionless pressure thrust was defined through two different manners. One is surface integral of two-dimensional pressure distribution (Eq. (3)), and the other is one-dimensional SAPD integral assuming no spanwise pressure variation (Eq. (4)). Each of them is normalized by surface area covering measurement locations symbolized as A_{RS} which is fixed value of 19000 mm^2 (see Fig. 3).

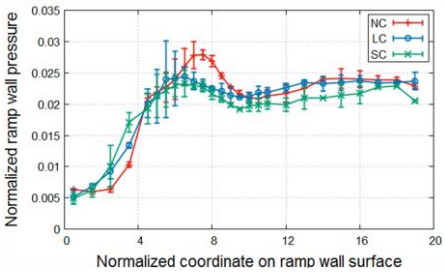

(a) NPR=26, over expansion condition

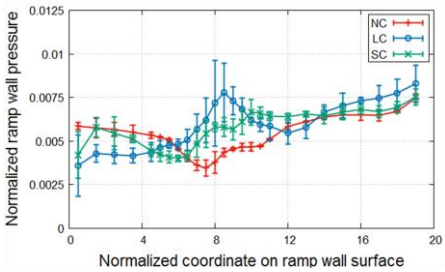

(b) *NPR*=87, under expansion condition

Fig. 4 Comparison of normalized streamwise pressure distribution among NC, LC, and SC test nozzles.

$$C_{p2D} = \frac{1}{p_{0n} \cdot A_{RS}} \sum_{i,j} p_w\left(\xi_i, y_j\right) \cdot A_{i,j} \tag{3}$$

$$C_{p1D} = \frac{1}{p_{0n} \cdot A_{RS}} \sum_{i,j} p_{wave}\left(\xi_i\right) \cdot A_{i,j} \tag{4}$$

The comparison between C_{p2D} and C_{p1D} evaluates the impact of spanwise variation in physical quantity on SEN thrust performance and necessity to consider the spanwise variation in performance prediction modeling.

3. Results and Discussion

3.1 Pressure distribution and coefficient

First, the pressure distribution is addressed. Again, we two-dimensionally measured the wall pressure distribution on test ramp, so that the pressure contour on test ramp was obtained through the present test. However, due to page limitation, the two-dimensional pressure contour is not addressed but only the one-dimensional SAPD is discussed. Figure 4 shows the SAPD (Eq. (1)) with error bar of standard deviation for spanwise pressure variation (Eq. (2)). The horizontal axis is streamwise coordinate on test ramp normalized with flow path exit height H_0 of LC or SC test nozzle that is 20 mm. The *NPR*s for cases Fig. 4 (a) and (b) are 26 and 87, so that each of them corresponds to the over and under expansion conditions, respectively.

The SAPDs were compared among NC, LC, and SC nozzle configurations under same *NPR*s. Since the cell base width for LC is larger than SC, the error bar became larger in the order of NC, SC, and LC. The NC had a slight pressure variation in spanwise direction, because of intrinsic non-uniformity brought by test facility. As for the over expansion condition (Fig. 4 (a)), the wall pressure distributions looked similar trend among NC, LC, and SC cases, so that the cell base existence and clustering manner should not manifestly affect the SEN ramp wall pressure distribution. The under expansion cases, on the other hand, had remarkable difference in wall pressure trend among NC, LC, and SC configurations. Regarding the NC case as a baseline, the LC case had larger difference than SC one. Unlike the NC and SC cases, first pressure change in LC case was increase. This should result from the wake flow formation in the cell base region. The wake flow accompanies the separated recirculation zone corresponding to the cell base area where the pressure is much smaller than that in surrounding flow. Such a low pressure region should significantly change the test nozzle exit condition, that is, the SEN entrance condition. Consequently, the LC and SC cases newly took the pressure distribution considering the change in the SEN entrance condition. Assuming the computation modeling, the entrance condition change can be translated into the input condition change. We had experimentally demonstrated that the SEN ramp wall pressure distribution strongly correlates to the *NPR* [5]. According to this fact, the input correction to change the *NPR* was proposed to reflect the cell base effect to the simulation.

Next is for the pressure coefficient, that is, dimensionless parameter evaluating the SEN thrust performance. The pressure coefficient variation with respect to *NPR* is given by Fig. 5. The results using each test nozzle is compared under same *NPR* by linear interpolation. Table 3 shows the pressure coefficient difference regarding the NC case as a reference under same *NPR*. Note that the pressure coefficient in this section is C_{p2D} (Eq. (3)). The pressure coefficient curves were almost same among NC, LC, and SC cases, and any differences did not exceed 10 %. These results should explain that the SEN pressure thrust is not so clearly affected by the cell base existence and clustering manner. Therefore, when only the SEN thrust has to be evaluated with precision

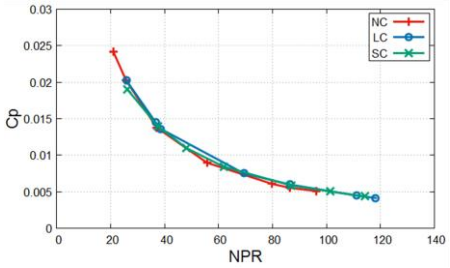

Fig. 5 Pressure coefficient versus *NPR*

Table 3 Pressure coefficient difference from NC to SC and LC cases

NPR	LC to NC, %	SC to NC, %
26	0.156	4.25
37	3.96	2.87
69	4.20	6.36
87	8.13	6.36
96	5.69	4.48

in conceptual design level, we may neglect the cell base existence and treat the nozzle as a non-clustered configuration.

3.2 Computational expression for cell base effect

To develop a SEN flow simulation model suitable for conceptual design phase, we discuss the application way of the cell base existence and clustering manner to the computation model. First, the difference between C_{p2D} and C_{p1D} is addressed. If the C_{p2D} to C_{p1D} difference is small enough to be neglected in the simulation modeling, we can estimate the C_{p2D} by deriving C_{p1D}. The C_{p2D} is regarded as a correct value to represent the SEN pressure thrust, because it is derived from surface integral of wall pressure actually acting on ramp surface. The C_{p1D} is, on the other hand, calculated through approximation on the ramp wall pressure from two- to one-dimensional distribution. This approximation process means the spatial averaging on the two-dimensional pressure distribution and then getting the one-dimensional SAPD. Figure 6 compares the C_{p2D} to C_{p1D} difference with respect to *NPR*. For the NC and SC cases, the discrepancy was only less than 0.5 %. The LC case had relatively large difference, but maximum one was still less than 1.2 %. We regarded these differences as negligibly small and concluded that the C_{p1D} can be employed as the prediction target for simulation model instead of C_{p2D}. In addition, these results should prove that the spanwise averaging on the ramp wall pressure distribution works well as one of the ways to reduce the computational model order. This should be because the spanwise well-organized flow is constructed in the SEN thanks to the symmetrical configuration even in clustered cases.

Next, based on aforementioned results, we discuss the input correction method to reflect the cell base existence and clustering manner to the computation model. The control volumes for the flow path exit and cell base regions are established along the streamline as shown in Fig. 7, so that *y*-directional length of total control volume becomes $w_{fe} + w_{cb}$. The character *w* means the width, and *fe* and *cb* represent the states in flow path exit and cell base regions before input correction, respectively. Figure 7 adopts the SC type test nozzle as a representative. The character *dx* in Fig. 7 denotes *x*-directional length of the control volume. Targeting these control volumes, mass, *x*-directional momentum, and energy of three conservation equations are formulated between each state in *ne* and *cb*, and *cr*. The character *cr* depicts the state after input correction. For simplicity, the following assumptions are made on formulating process. First one is that the single uniform flow in *cr* state is assumed to form as a result of the complete mixing within infinitesimal distance which is expressed as "$dx \rightarrow 0$" in Fig. 7. Second is that the quasi-one-dimensional flow is assumed in *x* direction, so that the physical quantities after instantaneous complete mixing, that is, *cr* state is constant in *z* and *y* direction. In this calculation, the calorically perfect gas is assumed, so that the specific heat ratio γ takes constant value for same substance. Definitional equation of speed of sound for calorically perfect gas is combined with equation of state, and as a result we get the velocity to Mach number transformation. Substituting this transformation into three conservation equations and arranging these equations for p_{cr} and M_{cr} give the following simultaneous equation.

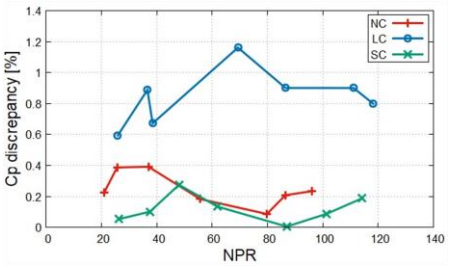

Fig. 6 Coefficients C_{p2D} to C_{p1D} difference with respect to *NPR*

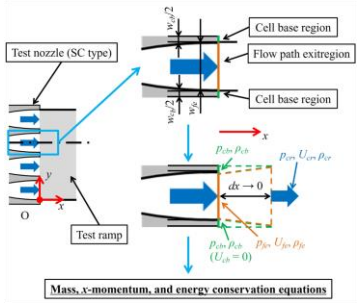

Fig. 7 Schematics illustrating input correction

$$\begin{cases} p_{cr} = \dfrac{w_{fe}}{w_{fe}+w_{cb}} \cdot p_{fe} \cdot \dfrac{M_{fe}}{M_{cr}} \cdot \sqrt{\dfrac{2+(\gamma-1){M_{fe}}^2}{2+(\gamma-1){M_{cr}}^2}} \\ M_{cr} = \sqrt{\dfrac{1}{\gamma}} \cdot \sqrt{\dfrac{w_{fe}}{w_{fe}+w_{cb}} \cdot p_{fe} \cdot \left(1+\dfrac{w_{cb}}{w_{fe}} \cdot \dfrac{p_{cb}}{p_{fe}} + \gamma {M_{fe}}^2\right) \cdot \dfrac{1}{p_{cr}} - 1} \end{cases} \quad (5)$$

The γ was fixed to be 1.4 in the present calculation, because the room temperature nitrogen was used for the test nozzle exhaust in the present experiment. Finally, we can obtain the p_{cr} and M_{cr} by solving Eq. (5).

For the computation, e.g. Computational Fluid Dynamics (CFD) simulation, the corrected pressure p_{cr} and Mach number M_{cr} can be directly utilized as one of the input parameters in boundary condition. To correlate the expansion condition defined by *NPR* with wall pressure distribution pattern, the corrected *NPR* symbolized by NPR_{cr} was also derived using p_{cr} and M_{cr}. The corrected value for test nozzle total pressure is calculated by isentropic deceleration from *cr* state to stagnation condition. Table 4 summarizes the input correction results. The Mach number change was relatively small, whereas the *NPR* significantly varies. We can confirm that the NPR_{cr} became less than 76, i.e. over expansion condition, even in the case of *NPR* larger than 76, i.e. under expansion condition. This should be one of the most remarkable effects of the cell base existence on the SEN thrust performance. In the future work, we will execute some simulations on the SEN flow adopting the aforementioned input correction. To do so, the CFD- or theory-based models are planned to be developed.

4. Conclusion

To characterize the effect of cell base width on SEN thrust performance and develop the way to reflect the cell base existence and clustering manner to computation model, the experimental investigation with wind tunnel test was performed. The present study principally revealed that the SAPD on SEN ramp wall varies corresponding to the cell base width and the clustering effect on the SEN thrust performance should be included in the simulation model by input correction which is flow unification through solving three conservation equations. Validity confirmation on the developed input correction will be conducted, as a future work, using CFD or physical model.

References

[1] Yoshida, M., Ishimoto, S., Kimura, T., Tomioka, S., Kodera, M. and Tani, K., "Future Space Transportation Vehicle Study at JAXA," *63rd International Astronautical Congress*, Naples, Italy, IAC Paper 15837, (2012).

[2] Javaid, K. H. and Serghides, V. C., "Airframe–Propulsion Integration Methodology for Waverider-Derived Hypersonic Cruise Aircraft Design Concepts," *Journal of Spacecraft and Rockets*, Vol. 42, No. 4, (2005), pp 663-671.

[3] Pittman, J. L., "A Mach 6 External Nozzle Experiment with Argon-Freon Exhaust Simulation," *SAE Transactions*, Vol. 98, (1989), pp 1683–91.

[4] Isono, T., Tomioka, S. and Sakaranaka, N., "An Experimental Investigation on Effect of Ambient Flow on Aerodynamic Performances of an External Nozzle," *Journal of Fluid Science and Technology*, Vol. 11, No. 1, JFST0002, (2016).

[5] Isono, T., Tomioka, S., Sakuranaka, N., Matsuo, A. and Mikoshiba, R., "An Experimental Study on Aerodynamic Characteristics of the External Nozzle in Clustered Airframe-Integrated Propulsion System Equipped with the RLV," *Aerospace Technology Japan*, Vol. 14, No. ists30, (2016), pp Pe_129-Pe_136.

Table 4 Test parameters through input correction

(b) LC case

NPR	NPR_{cr}	M_{fe}	M_{cr}
26	19	3.5	3.8
37	25	3.5	3.7
38	27	3.5	3.7
69	45	3.5	3.7
87	55	3.5	3.6
111	70	3.5	3.6
118	74	3.5	3.6

(a) SC case

NPR	NPR_{cr}	M_{fe}	M_{cr}
26	24	3.5	3.6
37	34	3.5	3.6
48	43	3.5	3.6
62	55	3.5	3.6
87	77	3.5	3.5
101	89	3.5	3.5
114	100	3.5	3.5